


DOI 10.24425/aee.2023.146047

# Measurement of combined gap in whole process of transmission lines' live working based on 3D laser point cloud

YING WANG<sup>1</sup> , HAITAO ZHANG<sup>1,2,3</sup>, QIANG LV<sup>3</sup>, QIANG GAO<sup>3</sup>, MINGXING YI<sup>3</sup>

<sup>1</sup>*School of Automation & Electrical Engineering, Lanzhou Jiaotong University  
Gansu, China*

<sup>2</sup>*Key Laboratory of Opto-Electronic Technology and Intelligent Control Ministry of Education  
Lanzhou Jiaotong University  
Gansu, China*

<sup>3</sup>*The UHV Company of State Grid Gansu Electric Power Company  
Gansu, China*

e-mail: [451739128@qq.com](mailto:451739128@qq.com)

(Received: 30.11.2022, revised: 28.04.2023)

**Abstract:** Transmission lines' live working is one of an effective means to ensure the reliable operation of transmission lines. In order to solve the unsafe problems existing in the implementation of traditional live working, the paper uses ground-based lidar to collect point cloud data. A tile based on the pyramid data structure is proposed to complete the storage and calling of point cloud data. The improved bidirectional filtering algorithm is used to distinguish surface features quickly and obtain a 3D model of the site. Considering the characteristics of live working, the speed of data reading and querying, the nearest point search algorithm based on octree is used to acquire a real-time calculation of the safe distance of each point in the planned path, and the safety of the operation mode is obtained by comparing with the value specified in the regulation, and assist in making decisions of the operation plan. In the paper, the simulation of the actual working condition is carried out by taking the "the electric lifting device ascending" as an example. The experimental results show that the established three-dimensional model can meet the whole process control of the operation, and has achieved practical effect.

**Key words:** 3D model, combined gap, laser point cloud, live working, transmission lines



© 2023. The Author(s). This is an open-access article distributed under the terms of the Creative Commons Attribution-NonCommercial-NoDerivatives License (CC BY-NC-ND 4.0, <https://creativecommons.org/licenses/by-nc-nd/4.0/>), which permits use, distribution, and reproduction in any medium, provided that the Article is properly cited, the use is non-commercial, and no modifications or adaptations are made.

## 1. Introduction

The northwest region of our country is located at high altitude, climate, terrain and other natural environmental factors are complex, as an important channel for power transmission, the EHV (abbreviation for “extra high voltage”) and UHV (abbreviation for “ultra-high voltage”) AC (abbreviation for “alternating current”)/DC (abbreviation for “direct current”) lines with a reliable power supply is extremely critical. Equipotential live operation is a non-power outage operation method to eliminate the defects and hidden dangers of transmission lines. It is very important to control the operation risk rate and analyze the risk factors [1].

Insufficient safety distance such as combination clearance in the live working process is easy to cause electric shock injury. The paths and ways of entering and leaving equipotential are different under different working environments and tower structures. The conventional operation methods are “soft ladder entering”, “the electric lifting device ascending” and “the hanging basket placing” [2].

Ensuring the relative safety of personnel is the key to live working, and all links in the process of site investigation, scheme formulation and operation implementation should be strictly controlled. In traditional, there are some problems such as inconsistency between actual working conditions on site and drawings, excessive reliance on manual labor in scheme formulation, prominent influence of personnel skills and experience, and difficulty in operation process control, which cannot meet the requirements of digital transformation and development of power grid [3].

Reference [4] proposes a density-based spatial clustering method aiming at the safety of power line distance from the ground, which performs least square linear fitting on laser point data after plane projection, and realizes fast segmentation and extraction of power line point cloud data with reference to empirical quantity to calculate the distance between the power line and ground object of the power corridor [4]. According to the hidden danger of the power line tree barrier, reference [5] extracted vectorized data of power line and convex points of vegetation based on elevation distribution characteristics and point cloud density characteristics to detect the hidden danger of the tree barrier [5]. Aiming at the detection of volume-specific tilt, reference [6] proposed to reduce the influence of other offset points on spatial straight line fitting by using the weight-iterative method of the robust estimation theory, and obtained the tilt of the tower by using the method that the center point of the rectangular geometry connected to the tower deviates from the actual central axis of the tower [6]. All the above algorithms have solved the actual problems in the field, but they all have certain limitations. They do not have control of the corresponding process variables, and cannot realize the warning, which is not conducive to the reliable operation of line equipment and the prevention and control of hidden dangers in advance.

On the basis of the above research, the flexible call of point cloud data and accurate measurement and analysis of safety distance have become the key to be studied according to the characteristics of dynamic changes in the live working process. The article will be based on a 3D laser point cloud, the accurate extraction of transmission line tower, wire, terrain and ground information, high precision reduction field information and combined with site safety rules and potential personnel in and out of the strong electric field, build the auxiliary decision-making system, measuring process safety distance and guiding live working site practice, as well as strictly control the safety of the operation site.

Section 2 describes the basic principle of point cloud acquisition and the steps of using a radar device to acquire a point cloud. Section 3 describes the organization and management of point cloud data, gross error elimination, classification and other processing methods and the nearest point search algorithm used. Section 4 describes the simulation and safety analysis of “the electric lifting device ascending”, and the simulation accuracy is verified.

## 2. Acquisition of point cloud data

A point cloud is the data collected by the lidar device with the measurement origin of the sensor center point as the geodetic coordinate and stored through its computing unit [7]. The scanning of ground objects such as poles and towers, metal tools, wires and insulators should be carried out in combination with the actual situation of the site, so as to ensure the acquisition of complete point cloud data and prepare for the next processing and application of the data.

In this paper, the ground station radar device is used for data acquisition [8]. The device adopts the pulse ranging method to calculate the distance between the radar and the line equipment by using the pulse interval between the laser point transmitting and receiving, and then obtains the three-dimensional point cloud data in the scene.

Figure 1 shows the method of obtaining point cloud data, and Fig. 2 shows the principle of lidar ranging.

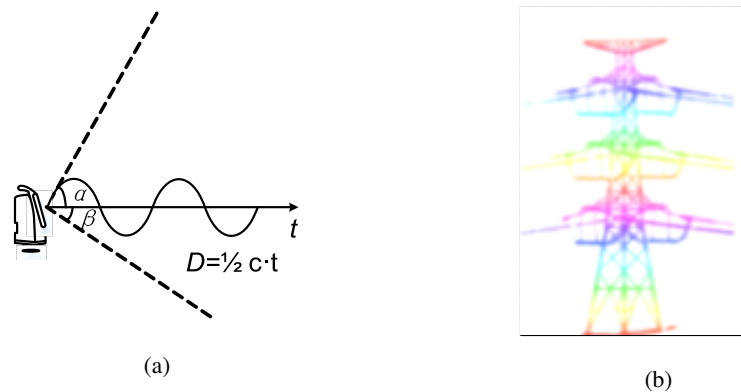


Fig. 1. Schematic diagram of pulse ranging

According to Fig. 1:

$$D = \frac{1}{2}ct, \quad (1)$$

where:  $t$  is the round trip time of the laser pulse,  $c$  is the speed of the laser in air, and  $D$  is the distance between the radar and the point to be measured.

Then, differentiate Eq. (1) and get Eq. (2) as follows:

$$\Delta D = c \times \Delta t, \quad (2)$$

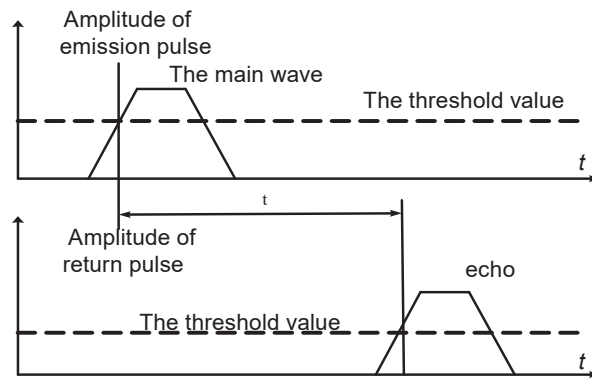


Fig. 2. Schematic diagram of scanning principle

where:  $\Delta D$  is the laser pulse ranging accuracy,  $\Delta t$  is the time measurement accuracy, and  $\Delta D$  is only relevant to  $\Delta t$ .

1. Considering that the actual propagation velocity of the laser in air is less than the speed of light due to the influence of water vapor, dust and other substances, increase the air dielectric constant correction  $\varepsilon$ , and the corrected distance calculation formula is as follows:

$$D = \frac{1}{2} \frac{c}{\varepsilon} t. \quad (3)$$

2. Considering that transmission tower structure has different heights due to the influence of height difference and voltage level, referring to the property of radar device's vertical scanning angle range of  $120^\circ$  and avoiding the problem of multi-point stacking after scanning directly against the tower, point scanning is generally carried out at  $45^\circ \sim 60^\circ$  along the road, and the closest distance between the foot of the nearest point at the bottom of the tower and the device is shown in the following equation:

$$L \geq \frac{H}{\tan 60^\circ}, \quad (4)$$

where:  $L$  is the distance between the measuring point and the foot of the nearest point tower,  $H$  is the distance between the ground wire and the horizontal base surface.

3. Considering the asymmetric structure of high and low legs of the tower affected by the tower topography, point cloud data scanning can cover the four tower foot direction point scanning at a certain angle along the line direction to the maximum extent.

The Polaris ground station lidar device was used for point cloud acquisition, and the data acquisition process was as follows:

1. Create and name a new project based on the job requirements.
2. Set point cloud data scanning parameters in a new project, including horizontal FOV (abbreviation for "field of view"), vertical FOV, Custom FOV, range mode, scanning result density, external camera, internal camera, continuous mode and so on. To ensure that the point cloud model is complete and the density meets the requirements, the vertical field angle is set to  $120^\circ$  and the scanning result density is set to medium density.

3. According to Formula (4) to determine the laser radar tower after the distance between the clockwise direction, in turn, determine the initial position and end position of the laser radar, then click the start button to start the radar screen device.
4. After the first point is scanned by  $45^\circ$  to  $60^\circ$  along the road, two times of tower point cloud data are obtained according to steps 1 to 3 in a clockwise direction of about  $120^\circ$  and  $240^\circ$  for later manual splicing of point clouds.

### 3. Processing of point cloud data

After the completion of point cloud data collection, in order to realize better implementation of the data, the large amount of original data and high density must be no topology structure of point cloud data processing, point cloud data structure configuration, convenient call, eliminate redundant data and extract the precise classification, provides a good condition for the live simulation precision measurement and safety distance analysis. In this paper, the data solving software supporting the ground laser measurement system is adopted. When used, the point cloud data in the geodetic coordinate system after registration can be automatically solved and generated by importing the obtained point cloud data, and the organization and processing of point cloud data can be realized synchronously.

#### 3.1. Organization and visualization of point cloud data

The point cloud data obtained in the operation has the characteristics of large quantity, high precision and rich detail expression. In order to strengthen the field practicability, facilitate data call, viewpoint update and data calculation, a hierarchical and block pyramid data organization algorithm of the point cloud is established in this paper according to the structure and characteristics of point cloud data, realizing intelligent storage and call of point cloud data, and dynamically loading appropriate data information according to user perspective information [9–11].

1. Firstly, the point cloud data is uniquely numbered,  $X_{\min}$ ,  $X_{\max}$  and  $Y_{\min}$ ,  $Y_{\max}$  that refers to the boundary range of point cloud data are obtained, and then the two-dimensional boundary range of the point cloud data is determined.
2. Next, specify the height – Tile\_Height – and the width – Tile\_Width – of the first or lowest unit tile and the drain factor between adjacent layers. Tile is a kind of overall organization structure representing data rows and columns, superimposed to form a pyramid structure with resolution from coarse to fine and data volume from small to large.
3. Then, calculate the total number of rows  $M$  and columns  $N$  of tiles in the first layer of the pyramid, as well as the two-dimensional range of each tile. The index coordinates of the pyramid tiles are  $L_K(ij)(i > j > 0)$ , of which  $\leq K \leq \text{Floor}_{\text{number}}$ . According to the point cloud data encoding in step 1, the range of  $i$  and  $j$  can be obtained as follows:

$$\begin{cases} 0 \leq i \leq (Y_{\max} - Y_{\min})/\text{Tile\_Height}/\text{Factor\_Value}^{K-1} + 1 \\ 0 \leq j \leq (X_{\max} - X_{\min})/\text{Tile\_Width}/\text{Factor\_Value}^{K-1} + 1 \end{cases}, \quad (5)$$

where: “/” is the rounding,  $i$ ,  $j$  is the row and column coordinates,  $K$  is the number of pyramid layers, and  $\text{Floor}_{\text{number}}$  is the total number of layers.

Thus, the range  $\text{Tile\_X}$  and  $\text{Tile\_Y}$  of each tile are calculated as:

$$\text{Tile\_X}_{\min} \leq \text{Tile\_X} \leq \text{Tile\_X}_{\max}, \quad (6)$$

$$\text{Tile\_Y}_{\min} \leq \text{Tile\_Y} \leq \text{Tile\_Y}_{\max}, \quad (7)$$

of which:

$$\begin{cases} \text{Tile\_X}_{\min} = X_{\min} + (j - 1) \times \text{Tile\_Width} \times \text{Factor\_Value}^{K-1} \\ \text{Tile\_X}_{\max} = X_{\min} + j \times \text{Tile\_Width} \times \text{Factor\_Value}^{K-1} \end{cases}, \quad (8)$$

$$\begin{cases} \text{Tile\_Y}_{\min} = Y_{\min} + (j - 1) \times \text{Tile\_Height} \times \text{Factor\_Value}^{K-1} \\ \text{Tile\_Y}_{\max} = Y_{\min} + j \times \text{Tile\_Height} \times \text{Factor\_Value}^{K-1} \end{cases}. \quad (9)$$

4. The length and width of the unit tile of the second layer are the  $\text{Factor\_Value}$  times that of the first layer. The range of the total number of rows, the total number of columns and the two-dimensional of each tile are calculated by the length and width of the unit tile of the layer. When  $\text{Factor\_Value} = 2$ , the following is the data storage structure diagram of each layer of the pyramid – Fig. 3.

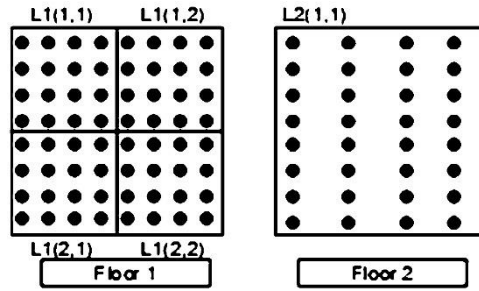


Fig. 3. Schematic diagram of data storage structure of each layer of point cloud pyramid

5. According to the algorithm, the tile structure of higher levels is generated until the whole original data are in the same tile, and the highest level  $N$  of the pyramid can be determined.
6. According to the determined two-dimensional boundary range of tiles of each layer, the original data is distributed to each tile of each layer of the pyramid from the bottom layer. The data at the bottom of the pyramid comes directly from the original data, the data of layer  $i + 1$  ( $i > 0$ ) is generated by the data of layer  $i$  [12, 13].
7. Each point in the original point cloud is traversed, which tile the point belongs to is judged according to the tile boundary of the layer, and the point number, point coordinates and point attributes are stored in the corresponding data file of the tile. The number of rows  $\text{Row}_{\text{count}}$  and columns  $\text{Column}_{\text{count}}$  in layer  $K$  is calculated according to the following formula:

$$\begin{cases} \text{Row}_{\text{count}} = (Y_{\max} - Y_{\min}) / \text{Tile\_Height} / \text{Factor\_Value} + 1 \\ \text{Column}_{\text{count}} = (X_{\max} - X_{\min}) / \text{Tile\_Width} / \text{Factor\_Value} + 1 \end{cases}. \quad (10)$$

8. Assign data to the pyramid tiles of the  $K + 1$  level. When assigning points, it only needs to determine whether the points in the corresponding  $K$  layer data tile meeting the conditions. The remaining tile data are allocated in the same way until the top level of the pyramid. The dilution factor set in the paper is 10.
9. 3D rendering of point cloud data [14]. Select the best pyramid level according to the position and angle of the user's viewpoint, and render tiles within the range of the projection polygon of the pyramid level according to the pyramidal perspective range.

When performing the zoom operation, select the tile of the higher layer. While, a denser layer of tiles is used for rendering. When the translation operation is performed, the original tile of the same level is cleared into memory synchronously and the new viewpoint window tile is loaded at the same time. Through the establishment of multi-layer data model, the speed of 3D scene rendering is improved.

### 3.2. Gross error removal of point cloud data

Affected by the position, angle and light of airborne lidar scanning, point cloud data will be overlapped, redundant and distorted. Therefore, in the case of retaining useful point cloud data, the number of points should be controlled by eliminating the gross error of point cloud data [15]. Considering the redundant data will interfere with the safety analysis of live working in the next step. Therefore, on the basis of manual clipping, the gross error is automatically eliminated.

Whether a point  $p$  in the point cloud is retained, the elevation  $Z'$  of this point is interpolated through the surrounding points, and then the difference between the elevation  $Z'$  and the elevation of the point  $p$  is calculated. If the value is greater than a certain limit  $\varepsilon$ , the point elevation will be eliminated. Distance-weighted average interpolation is used in this paper. The specific formula is as follows:

The square of the distance  $d_i$  from the surrounding point to the point  $p$  is:

$$d_i^2 = (x - x_i)^2 + (y - y_i)^2. \quad (11)$$

The value of the distance weighting function is:

$$c_i = 1 / (d_i^2 + e). \quad (12)$$

The elevation interpolation of point  $p$ :

$$Z_i = \frac{\sum_{i=1}^n c_i Z_i}{\sum_{i=1}^n c_i}. \quad (13)$$

When  $Z' - Z \geq \varepsilon$ , the point cloud would be abandoned.

The value  $\varepsilon$  in the above equation is determined based on the flatness of the ground surface, ranging from 0.02 to 0.1. In order to ensure the accuracy of interpolation results, the circular area points with  $p$  as the center and  $D$  as the radius are selected to participate in the calculation of  $Z'$ .

In the process of calculation, firstly calculates the number of point clouds in the circle, and then goes through them in turn to judge the situation of adjacent point clouds.

Figures 4 and 5 show the effect of eliminating gross errors for stage line data. The first figure shows the original point cloud data, and the second figure uses parameters with the number of nearest neighboring points being 3 and the standard deviation being 10. After the execution, some flying points in the air are removed after eliminating gross errors.

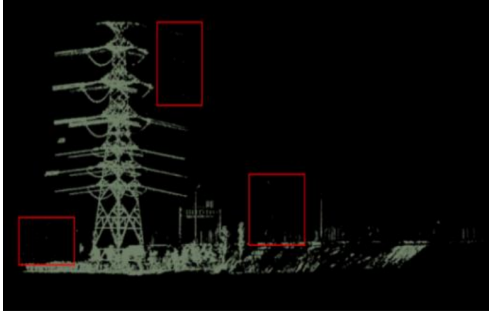


Fig. 4. Schematic diagram before elimination



Fig. 5. Schematic diagram after elimination

### 3.3. Classification of point cloud data

After the above processing, the point cloud is still a series of irregular points, which doesn't meet the practical application. It is necessary to classify the point cloud data and extract the ground and ground object information accurately from the discrete point cloud, so as to provide more effective information for the safety analysis of live work [16, 17]. In this paper, the point cloud classification algorithm is studied to automatically separate the point cloud into ground object points and ground points.

For any point  $p_i$  of the point cloud data, if the elevation difference  $dZ_i$  is less than a given threshold  $\text{Limit\_dZ}$  in the neighborhood of  $p_i$ , and the slope  $\text{Slope}_i$  is less than its given threshold  $\text{Limit\_Slope}$ , then  $p_i$  is considered as a ground object point; otherwise, it is a ground point. The classification function is:

$$\text{Point}_i(p_i) = \begin{cases} 0, & dZ_i < \text{Limit}_{dZ}, \text{ Slope}_i < \text{Limit\_Slope} \\ 1, & \text{else} \end{cases}, \quad (14)$$

where 0 indicates the ground object point, and 1 indicates the ground point.

According to this method, each point on the scan line is assigned with two identification markers  $aiLtoR$  and  $aiRtoL$ , which are respectively used for the ground object point and the ground point of the temporary identification. The data were processed and marked along the scan line in both positive and negative directions, and the results of the two scans were integrated. If  $aiLtoR$  and  $aiRtoL$  of point  $p_i$  are both marked as 0, then  $p_i$  is a ground object point. And if either  $aiLtoR$  and  $aiRtoL$  of point  $p_i$  is marked as 1, then  $p_i$  is a ground point. As follows:

$$\text{Point}(P_i) = \begin{cases} 0, & aiLtoR + aiRtoL = 0 \\ 1, & \text{else} \end{cases}. \quad (15)$$



However, the idea of this one-dimensional bidirectional filtering algorithm has some shortcomings. That is, the first point of the forward filtering mark cannot be artificially accurately determined which kind of point it belongs to, and the first point of the reverse filtering mark cannot artificially determine its type, which easily leads to the inaccurate results obtained by the two filterings [18]. Aiming at this problem, this paper formulates improvement measures: according to whether the elevation difference between the left, right points and the point exceeds the given threshold, then determining whether the point is extremely low. If it is, excluded, otherwise, it is a ground object. Then, according to the ground object point that has been determined, the slope and elevation difference are filtered to the left and right sides. The specific algorithm is as follows.

The data is divided into many scan lines along the  $Y$ -axis, and the ground object points in the scan lines are found by the above methods. Then the data in the scan line are filtered by the method based on slope. The slope of two adjacent points can be calculated as follows:

$$\text{Slope}_i = \frac{Z_i - Z_{i-1}}{\sqrt{(X_i - X_{i-1})^2 + (Y_i - Y_{i-1})^2}}. \quad (16)$$

When the absolute value of slope  $\text{Slope}_i$  of point  $P_i$  meets the given threshold, the attribute of point  $P_i$  will be judged according to whether point  $p_{i-1}$  is a ground point. Otherwise, calculate whether the height difference between point  $p_i$  and point  $p_{i-1}$  meets the given threshold. If it does, it is the ground object point. On the contrary, it is the ground point.

In addition, when the absolute value of slope  $\text{Slope}_i$  at point  $P_i$  does not meet the given threshold.

When  $\text{Slope}_i <$ , the classification function is:

$$\text{Point}(P_i) = \begin{cases} 0, & (P_{i-1} = 0, Z_i - Z_t < \text{Lim } t_H) \\ \text{or} & (P_{i-1} = 1, Z_i - Z_t > \text{Lim } t_H) \\ 1, & (P_{i-1} = 0, Z_i - Z_t \geq \text{Lim } t_H) \\ \text{or} & (P_{i-1} = 1, Z_i - Z_t \leq \text{Lim } t_H) \end{cases}, \quad (17)$$

where:  $Z_t$  is the elevation of the nearest ground point from point  $p_i$ ,  $\text{Lim } t_H$  is the given elevation difference threshold.

When  $\text{Slope}_i >$ , the classification function is:

$$\text{Point}(P_i) = \begin{cases} 0, & P_{i-1} = 0, Z_i - Z_t < \text{Lim } t_H \\ 1, & P_{i-1} = 0, Z_i - Z_t \geq \text{Lim } t_H \text{ or } P_{i-1} = 1 \end{cases}. \quad (18)$$

The above algorithm can filter out the ground points and obtain the ground object points.

According to the above methods, point cloud data can be classified as ground object points and ground points. For incorrectly classified point cloud data, manual interaction can also be used to set, and then manually distinguish tower, insulator string, jumper, ground wire, wire, ground and vegetation by marking different colors [19]. In Fig. 6, the following is the effect drawing of component classification and extraction of 750 kV tensioning tower and whole transmission wire completed based on the above method. Field practice shows that this method is also suitable for other voltage levels of transmission lines.

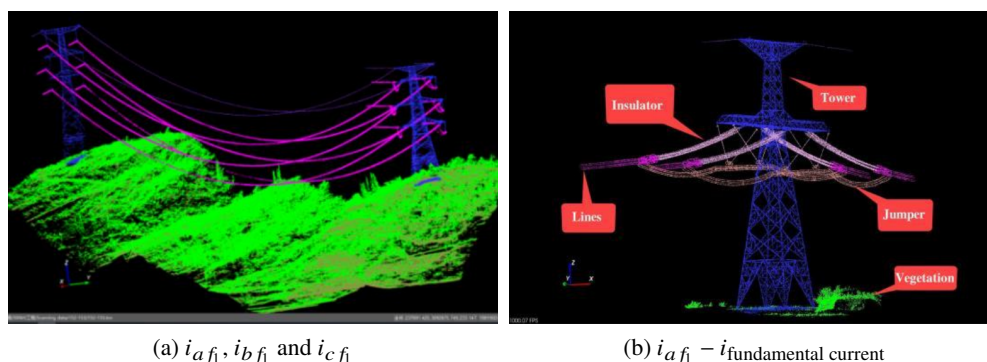


Fig. 6. Schematic diagram of point cloud classification effect

### 3.4. The nearest point search algorithm

Combined with the rapid calculation, convenient and practical engineering needs and live working must meet the characteristics of minimum safety distance. It is necessary to find the nearest point from the center of the human body in the obtained point cloud data, accurately obtain the spatial closest distance, and further verify the feasibility of the operation method [20]. In order to achieve selective point cloud data processing and improve the efficiency of operation, the following will focus on the research of an octree data structure based on a spatial index, and use the nearest point search algorithm to find the nearest point in the point cloud space.

The closest point search means that a set of points  $S$  and a target point  $q$  are given in a scale space  $M(q \in M)$ , and then find the closest point to  $q$  in  $S$  [21].

According to the octree structure, after the point cloud data is stored, when the nearest point of a point cloud needs to be found, only the points in the voxel where the point cloud is located and the surrounding neighboring voxels need to be found, which is conducive to search data efficiently, retrieve and modify the translated results fast [22]. The specific implementation steps are as follows:

1. Set the maximum recursion depth.
2. Find the maximum size of the scene and build the first cube with that size.
3. Drops the identity elements into a cube that can be contained and has no child nodes of the cube.
4. If the maximum recursion depth is not reached, continue to subdivide it into eight equal parts and repeat step 3 until the maximum recursion depth is reached. When the number of unit elements assigned to the sub-cube is not zero and is the same as the parent cube, the sub-cube stops subdividing.

The following is to search and test the nearest point of the octree. Table 1 shows the times using the original lookup method and octree lookup method for finding the nearest point to a specified point (set) from multiple points, and the octree search time does not include the process of establishing the octree. The data in the table show that the search speed based on octree increases slowly, but the search speed is relatively fast.

Table 1. Time comparison of nearest point search algorithm

| The number of points in point set 1 | 1       | 1         | 1         | 12 704    | 59 821      |
|-------------------------------------|---------|-----------|-----------|-----------|-------------|
| The number of points in point set 2 | 242 505 | 1 047 319 | 5 778 522 | 61 719    | 1 047 319   |
| Times of original method            | 2 mms   | 15 mms    | 37 mms    | 4 525 mms | 362 286 mms |
| Times of octree lookup              | < 1 mms | < 1 mms   | 1 mms     | 20.2 mms  | 57 569 mms  |

## 4. Methods' simulation and security analysis

After the 3D model generation, we can simulate the whole process of the live working, and be familiar with the operation process in advance. At the same time, we found hidden security trouble in the established plan [23]. In the paper, “the electric lifting device ascending” is simulated, and the algorithm is used to calculate the combined gap accurately, meanwhile, the combined gap in the process of operation is analyzed [24, 25], then compared with the safety value required by the rules to determine whether it is safe.

### 4.1. Method simulation

“The electric lifting device ascending” is a live working mode in which the operator is assisted by the electric lifting device from the ground vertically to the operating point of the wire. The minimum combined gap among the operator, the ground body (tower) and live body (conductor) during the operation must meet the requirements of the safety regulations [26], at the same time, the backup protection rope of equipotential personnel must be connected to the backup high strength insulation rope. The specific simulation process is as follows:

1. Determine the location of defects and make pre-selection plans;
2. Set the high strength insulation rope hanging point and the initial position of the operator. According to the symmetry characteristics of the tower, the point cloud data angle is adjusted to ensure that the two points are located in the same vertical plane;
3. Taking the initial position of the operator as the starting point, the operator entry path, namely the detection path, is set up between the operator and the insulation rope hanging point;
4. Set the simulated person to move along the established path to complete the construction simulation.

### 4.2. Safety analysis

Figure 7 shows the whole process simulation diagram of “the electric lifting device ascending”. In Fig. 7, mark the simulated person at the green dot ①, ② and ③, and the distance between the person, the tower and the wire are indicated by green and yellow line segments respectively. This is according to the regulations:

$$L = S_{\text{green}} + S_{\text{yellow}} . \quad (19)$$

In Eq. (19),  $L$  is the combined gap of the simulated figure at this point. According to the above simulation process, the software synchronization begins to detect each point in the path. The specific steps are as follows:

1. According to the detection step size, calculate the total number of detection steps and confirm the detection point;
2. Each detection point was cycled along the detection trajectory, and the combined gap  $L$  was calculated based on the consideration of the human body occupying no less than 0.5 mm [26].
3. Obtain the minimum combined gap  $L_{\min}$  at the voltage level and altitude from the safety procedure and judge the safety.
4. After the above safety test is completed, the test result will be generated immediately.

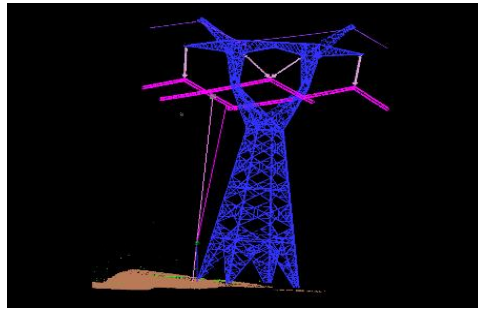


Fig. 7. Schematic diagram of the whole process simulation

#### 4.3. The test results

In order to ensure that the personnel occupation is not less than 0.5 mm, and the actual operation process has enough safety margin, In the process of method simulation, as shown in Fig. 8, the operator is simulated as a cuboid, and in the figure, point  $o$  represents the personnel center of gravity,  $ae$  is the width of the personnel,  $ad$  indicates the personnel thickness. The personnel height is represented by the sum of the height  $ac$  above the center of gravity and the height  $ab$  below the center of gravity. Finally, parameters are set according to the actual

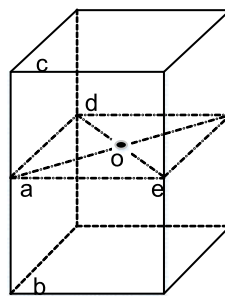



Fig. 8. Diagram of personnel model

situation. The detection process traverses each point on the cuboid, calculating the minimum distance  $S_{\text{yellow}}$  to the charged body and the minimum distance  $S_{\text{green}}$  to the ground body, then the minimum combined gap  $L$  of this point is obtained.

The security of the midpoint of the path is judged by cyclic detection in the process of security analysis. When  $L < L_{\text{min}}$ , it indicates that the point is dangerous, otherwise safe. As shown in Table 2, when a point in the simulation path meets the safety value required by the regulations, it is automatically marked as green. When a point does not meet the requirements of live work, it is automatically marked as a red alert.

Table 2. Statistics of detection results

|  |   | Difference with regulation (m) | Combined gap (m) | Minimum distance with ground body (m) | Minimum distance with charged body (m) |
|--|---|--------------------------------|------------------|---------------------------------------|--|
|  | 1 | 41.6249                        | 46.5249          | 44.6265                               | 1.89842                                |
|  | 2 | 41.6834                        | 46.5834          | 40.7038                               | 5.8796                                 |
|  | 3 | 41.7522                        | 46.6552          | 35.8079                               | 10.8455                                |
|  | 4 | 35.2554                        | 40.1554          | 25.0584                               | 15.0969                                |

Based on the above research, when the danger point appears in the simulated path, besides the marking prompt, the danger point information given by the algorithm also includes the coordinates of the danger point, the minimum distance from the danger point to the ground body, the minimum distance from the danger point to the live body, and the numerical difference from the minimum combined clearance specified in the regulations. After the path simulation is completed, the software generates the detection scheme according to the result of the path security detection.

#### 4.4. Accuracy verification

To verify the measurement accuracy of point cloud data in the simulation of the above working conditions, the simulation scenario is specially set. Then using the total station (angle measuring accuracy  $2''$ , ranging accuracy  $3 \text{ mm} \pm 2 \times 10^{-6} D$ ) to determine the insulation rope hanging point and the initial actual position of the personnel in the detection scheme, and it is determined that the measured environment is consistent with the simulated environment. Then use the laser rangefinder (Leica D810, ranging accuracy  $\pm 1 \text{ mm}$ ) to select three points in the operational path to collect coordinate data, and the distance from the geometric center of the electric lifting device, which is marked before the job, to the tower and the nearest part of the wire is screened and measured, then the combined gap will be calculated. The actual operation diagram is shown in Fig. 9.

When the above condition is simulated, for the convenience of calculation and check, we set the width, thickness and height of the personnel model shown in Fig. 9 as the minimum value  $0.01 \text{ mm}$  (it is approximately a point), and search three points A, B and C whose coordinates match those collected in the actual operation process in the point cloud path, of which the corresponding



Fig. 9. Schematic diagram of practical operation

coordinate error value  $xyz$  of the point is no more than 0.005 mm. Based on these, the combined gap can be calculated, then compared with the data acquired by the rangefinder, the relative error is obtained. Both the simulated and measured data and calculation results obtained from the above three points are shown in Table 3.

Table 3. Comparison of combined clearance measurements

| Collected points | Simulated value (m) | Measured value (m) | Relative error (m) |
|------------------|---------------------|--------------------|--------------------|
| <b>A</b>         | 11.6127             | 11.665             | -0.0523            |
| <b>B</b>         | 10.4782             | 10.527             | -0.0488            |
| <b>C</b>         | 9.83448             | 9.889              | -0.05452           |

The results show, the measurement errors of the combined gap are all within the range of 0.06 mm, which meets the requirement that the range of human activity in the safety regulations is not less than 0.5 mm. Considering the high density of point cloud data and the human error in the measurement, the results of laser radar device and laser rangefinder are consistent, and meet the requirements of to the data accuracy to the live working process. At the same time, the application of the software in practice shows that this method realizes the process control of live work. It avoids the disadvantage of relying too much on experience in process management, and improves the efficiency and safety of work on site.

## 5. Conclusions

Through the theoretical research and practical application, the auxiliary measurement of the combined gap in live working based on laser point cloud data is proposed, and draws the following conclusions:

1. Through the visualization organization, gross error elimination, fine classification, nearest point measurement of point cloud data, the combination of theoretical research and engineering practice has been realized, and theoretical experience has been accumulated for reasonable organization, efficient invocation, and practical use of point cloud data in the field of transmission in the future.
2. Through the simulation of “the electric lifting device ascending”, realizes the scientific simulation of a live working process under the condition of complex working procedure and difficult safety control, it provides a reliable basis for the actual work and has reference value for the simulation of other construction methods.
3. Through 3D simulation, the operation path of equipotential personnel is determined, the safety of the operation process is controlled in real time, and the safety margin of the operation process is intuitively and efficiently displayed for the operators.
4. Through practical application, it is verified that the proposed method has great promotion value in the engineering field, and has positive significance in promoting the ability improvement of the grass-roots team and the intelligent assisted transformation of the field work.
5. Further research focus, through combining the developed software with the actual operation, the personnel carry the differential positioning device to display the safe distance of each point in the path and in real time under the real condition, which will be realized.

### Acknowledgments

This work was jointly supported by National Natural Science Foundation of China Regional Project (52067013); Natural Science Key Foundation Project of Science and Technology Department of Gansu Province (21JR7RA280); Natural Science Foundation of Gansu Province (22JR5RA318); The cost project of Gansu Power Grid (B127452200D1).

### References

- [1] Li R.H., *Analysis of the hazard rate and accident rate of live work*, Power Safety Technology, vol. 19, no. 2, pp. 41–43 (2017).
- [2] Tan Y.D., Wang X.X., *Introduction to the way of entering the equipotential for live work*, Power Grid Technology, no. 6, pp. 30–33 (2021).
- [3] Zhang X.Q., Guo W.P., *Innovation and practice of digital team construction in power grid enterprises*, Innovation World Weekly, no. 4, pp. 70–80 (2021).
- [4] Shi L., Guo T., *Research on segmentation and security detection of power line laser point cloud*, Laser Technology, vol. 43, no. 3, pp. 341–346 (2019).
- [5] Wu Z.R., Fan L.M., *Rapid detection method for hidden danger of transmission line tree barrier based on airborne laser point cloud*, Applied Laser, vol. 43, no. 3, pp. 128–134 (2022), DOI: [10.14128/j.cnki.al.20224203.128](https://doi.org/10.14128/j.cnki.al.20224203.128).
- [6] Xu L.G., Shi L., *A transmission line tower tilt detection algorithm based on laser point cloud*, Laser Technology, vol. 46, no. 3, pp. 390–396 (2022).
- [7] Wang J., Zhang J., *Research on 3D laser scanning technology based on point cloud data acquisition*, 2014 International Conference on Audio, Language and Image Processing, Shanghai, China, pp. 631–634 (2014).

- [8] Xiong Y.Y., Qiao J.G., Zhang W.J., *Fisheye image and ground lidar point cloud registration based on line features*, Bulletin of Surveying and Mapping, no. 7, pp. 74–80 (2021), DOI: [10.13474/j.cnki.11-2246.2021.0212](https://doi.org/10.13474/j.cnki.11-2246.2021.0212).
- [9] Tao S.B., Liang C., *Sparse voxel pyramid neighborhood construction and classification of LiDAR point cloud*, Journal of Image and Graphics, vol. 26, no. 11, pp. 2703–2712 (2021).
- [10] Hui L., Yang H., *Pyramid Point Cloud Transformer for Large-Scale Place Recognition*, 2021 IEEE/CVF International Conference on Computer Vision (ICCV), Shanghai, China, pp. 6078–6087 (2021).
- [11] Zeng X.Z., Li C.R., *Research on Superimposition Pyramid Index Applied to Massive Points Cloud Fast Display*, Remote Sensing Technology and Application, vol. 30, no. 3, pp. 534–539 (2015).
- [12] Wang H.P., Zhang C.S., *Applicability analysis of thinning algorithm for point cloud data of transmission line corridors*, Science of Surveying and Mapping, vol. 45, no. 9, pp. 152–158 (2020), DOI: [10.16251/j.cnki.1009-2307.2020.09.023](https://doi.org/10.16251/j.cnki.1009-2307.2020.09.023).
- [13] Prio M.H., Patel S., *Implementation of Dynamic Radius Outlier Removal (DROR) Algorithm on LiDAR Point Cloud Data with Arbitrary White Noise Addition*, 2022 IEEE 95th Vehicular Technology Conference: (VTC2022-Spring), Helsinki, Finland, pp. 1–7 (2022), DOI: [10.1109/VTC2022-Spring54318.2022.9860643](https://doi.org/10.1109/VTC2022-Spring54318.2022.9860643).
- [14] Munir N., Awrangjeb M., *Extraction of Forest Power lines From LiDAR point cloud Data*, 2021 Digital Image Computing: Techniques and Applications (DICTA), Gold Coast, Australia, pp. 1–6 (2021), DOI: [10.1109/DICTA52665.2021.9647062](https://doi.org/10.1109/DICTA52665.2021.9647062).
- [15] Hao G., Hu X.F., *A preprocessing method for 3D laser scanning point cloud data*, Science of Surveying and Mapping, vol. 39, no. 7, pp. 90–93 (2014), DOI: [10.16251/j.cnki.1009-2307.2014.07.017](https://doi.org/10.16251/j.cnki.1009-2307.2014.07.017).
- [16] Itakura K., Miyatani S., *Estimating Tree Structural Parameters via Automatic Tree Segmentation from LiDAR Point Cloud Data*, IEEE Journal of Selected Topics in Applied Earth Observations and Remote Sensing, vol. 15, pp. 555–564 (2022), DOI: [10.1109/JSTARS.2021.3135491](https://doi.org/10.1109/JSTARS.2021.3135491).
- [17] Ma D.L., Wang X.K., *A point cloud data classification method based on height difference*, Bulletin of Surveying and Mapping, vol. 8, no. 6, pp. 46–49 (2018), DOI: [10.13474/j.cnki.11-2246.2018.0174](https://doi.org/10.13474/j.cnki.11-2246.2018.0174).
- [18] Zhao J.H., Dou X.T., *A method for 3D point cloud classification based on segmentation results*, Science of Surveying and Mapping, vol. 47, no. 3, pp. 85–95 (2022), DOI: [10.16251/j.cnki.1009-2307.2022.03.012](https://doi.org/10.16251/j.cnki.1009-2307.2022.03.012).
- [19] Zhou W., Peng C.C., *LIDAR point cloud texture feature extraction method*, Journal of National University of Defence Technology, vol. 41, no. 2, pp. 124–131 (2019).
- [20] Zhou R.Q., Xu Z.H., *An airborne laser point cloud classification method for high-voltage power transmission corridors*, Science of Surveying and Mapping, vol. 44, no. 3, pp. 22–27 (2019), DOI: [10.16251/j.cnki.1009-2307.2019.03.004](https://doi.org/10.16251/j.cnki.1009-2307.2019.03.004).
- [21] Jia Y., *Design of nearest neighbor search for dynamic interaction points*, 2021 2nd International Conference on Big Data and Informatization Education (ICBDIE), Hangzhou, China, pp. 389–393 (2021).
- [22] Bai Y., Tang W., *Real-time and high-precision ranging method for large dynamic range of imaging lidar*, Infrared and Laser Engineering, vol. 49, no. S2, pp. 1–6 (2020).
- [23] Wang Y. et al., *Elastic and Efficient LiDAR Reconstruction for Large-Scale Exploration Tasks*, 2021 IEEE International Conference on Robotics and Automation (ICRA), Xi'an, China, pp. 5035–5041 (2021), DOI: [10.1109/ICRA48506.2021.9561736](https://doi.org/10.1109/ICRA48506.2021.9561736).
- [24] Wang Y.J., Lian T.F., *Point cloud registration method based on octree and KD tree index*, Surveying and Mapping Engineering, vol. 26, no. 8, pp. 35–40 (2017), DOI: [10.19349/j.cnki.issn1006-7949.2017.08.008](https://doi.org/10.19349/j.cnki.issn1006-7949.2017.08.008).



- [25] Wen Y.W., Deng C.Y., *Application of 3D laser scanner in actual measurement of electric power engineering*, Bulletin of Surveying and Mapping, no. 10, pp. 163–167 (2021).
- [26] Zhang Q.S., Wang L.N., *Simulation and analysis method of gap discharge characteristics of live work combination*, High Voltage Technology, vol. 44, no. 4, pp. 1293–1301 (2018), DOI: [10.13336/j.1003-6520.hve.20180329032](https://doi.org/10.13336/j.1003-6520.hve.20180329032).
- [27] Wang L.N., Hu Y., *Discharge mechanism of combined gaps in live operation of UHV transmission lines*, High Voltage Technology, vol. 37, no. 5, pp. 1224–1230 (2011), DOI: [10.13336/j.1003-6520.hve.2011.05.023](https://doi.org/10.13336/j.1003-6520.hve.2011.05.023).
- [28] State Grid Corporation of China, Q/GDW1799.2, *State Grid Corporation Electric Power Safety Work Regulations (Line Part) [S]*, Beijing (2013).